Absolute Age and Temperature Constraints on Faulting along the Basal Décollement of the Jura Fold-and-thrust Belt from Carbonate U-Pb Dating and Clumped Isotopes

N. Looser[1], H. Madritsch[2], M. Guillong[1], O. Laurent[1], S. Wohlwend[1], and S. M. Bernasconi[1]

[1] Department of Earth Sciences, ETH Zurich, Sonneggstrasse 5, 8092 Zurich, Switzerland

[2] Swiss National Cooperative for the Disposal of Radioactive Waste (Nagra), Hardstrasse 73, 5430 Wettingen, Switzerland.

Corresponding author: Nathan Looser (nathan.looser@erdw.ethz.ch)

Key Points:

- Propagation of Alpine deformation along the basal décollement into the distal foreland initiated at ~14.3 Ma at the latest
- Deformation occurred over a time period of at least ~10 Ma (14.3-4.5 Ma) with contemporaneous activity of thrusts and strike-slip faults
- Constant in-situ temperatures and fluid sources over the recorded time period show that large-scale foreland erosion initiated after ~4.5 Ma

Abstract

During its late-stage evolution, the European Alpine orogen witnessed a northwest-directed propagation of its deformation front along an evaporitic basal décollement into the foreland. This resulted in the decoupling of the northern Alpine Molasse Basin from its basement and the formation of the Jura fold-and-thrust belt. Here, we present the first absolute age and temperature constraints on deformation along this basal décollement using combined carbonate U-Pb LA-ICP-MS dating and clumped isotope thermometry. We analyzed calcite veins associated with a thrust fault branching off from the basal décollement in the distal Molasse Basin and slickenfibers from thrusts and strike-slip faults in the eastern Jura Mountains. Our U-Pb data provide evidence for tectonic activity related to Alpine contraction in this region between ~14.5 Ma and ~4.5 Ma ago. Accordingly, the propagation of Alpine deformation into the distal foreland along the basal décollement occurred earlier than commonly inferred by biostratigraphy, at Middle Miocene (Langhian) times at the latest. Younger deformation ages between ~11.5 and ~4.5 Ma correspond very well in time with shortening in the Subalpine Molasse and the Central Alps proving simultaneous tectonic activity along both thrust fronts; e.g. the Jura Mountains and the Subalpine Molasse. Clumped isotopes reveal vein calcite precipitation at temperatures between 53 and 104 °C from fluids with oxygen isotope compositions between -6.2 and +9.5 ‰. Our data show that the burial conditions in the studied area remained constant between ~14.5 Ma and ~4.5 Ma indicating that the previously reported large-scale foreland erosion initiated after ~4.5 Ma.

1 Introduction

The timing of formation and the deformation sequence of foreland fold-and-thrust belts provide fundamental constraints for geodynamic reconstructions of convergent orogens (Poblet and Lisle, 2011; Pfiffner, 2017). Besides the timing, the temperature conditions and fluid flow during deformation are further key parameters for understanding foreland fold-and-thrust belt evolution as the kinematics of viscous décollement-based thrust systems is known to be strongly governed by temperature and fluid circulation (e.g. Nemcok et al., 2009). The most direct way to derive these key parameters is to access carbonate cements that precipitated in veins related to the foreland thrust system during times of tectonic activity. Recent progress in carbonate U-Pb LA-ICP-MS geochronology have opened new perspectives in unravelling complex, multiphase deformation histories (e.g. Beaudoin et al., 2018; Parrish et al., 2018). Clumped isotope thermometry, on the other hand, has proven itself as a valuable tool to reconstruct temperatures and fluid flow during fault movement (e.g. Huntington and Lechler, 2015; Fernandez et al., 2017; Smeraglia et al., 2020). In this study, we use combined carbonate U-Pb LA-ICP-MS dating and clumped isotope thermometry (e.g. Mangenot et al., 2018) on calcite veins to constrain thrusting along the basal décollement of the Jura Mountains, a classic fold-and-thrust belt example in the northwestern foreland of the European Alps.

The formation of the Jura Mountains is coupled to the late stage evolution of the Alpine orogen and is associated with a northwest directed propagation of the Alpine front of up to 80 km into the foreland (Figs. 1a and 1b; Laubscher, 1978; Pfiffner, 1986; Burkhard, 1990). It is related to Miocene upper crustal nappe stacking in the Central Alps due to plate convergence (“distant push” hypothesis; Buxtorf, 1907; Laubscher, 1978). Deformation into the foreland propagated in a thin-skinned manner along a shallow dipping thrust décollement constituted by rheologically weak Triassic evaporites near the base of the Mesozoic succession underneath the

Tertiary Molasse Basin (Figs. 1b and 1c, Philippe et al., 1996; Sommaruga et al., 2017). The basal décollement comprises two main levels that are located within the evaporitic successions of the Triassic Keuper and Muschelkalk groups. Deformation associated with the décollement occurs in both levels as well as connecting the two levels (Sommaruga et al., 2017 and references therein). During or slightly after the formation of the Jura Mountains, the Molasse Basin experienced inversion and km-scale erosion. The exact timing of the onset and the amount of erosion is under debate (Cederbom et al., 2004; Mazurek et al., 2006; Von Hagke et al., 2012).

To date, no absolute and direct age and temperature data for thrusting along the basal décollement exist. Timing constraints for the formation of the Jura Mountains are sparse and mostly based on relative age constraints stemming from locally preserved Tertiary deposits showing signs of deformation and being dated by biostratigraphy. Seismic observations in the most distal part of the foreland basin and the youngest Molasse deposits found in synclines of the Jura Mountains suggest that the main phase of folding in this area occurred after ~12 Ma (Sommaruga et al., 1995; Becker, 2000 and references therein; Malz et al., 2016). Along the northern margin of the Jura Mountains, biostratigraphic ages of Tertiary deposits in synclines and over-thrusted Tertiary deposits north of the Jura frontal thrust suggest a maximum age for northernmost folding and frontal thrusting of ~11 Ma (Kälin, 1997). A Minimal age of ~3 Ma for folding in the Jura mountains was derived based on undeformed (post-folding) karst infills (Bolliger et al., 1993). A similar time frame of ~9-3 Ma was suggested for frontal thrusting along the western Jura margin along the Bresse Graben (Becker, 2000 and references therein). Notably, some authors have argued for a much earlier onset of Alpine foreland thrusting in the western proximal Molasse Basin based on the interpretation of syntectonic Early Miocene (Burdigalian, ~20-16 Ma) Molasse sediments located close to the Alpine front (Deville et al., 1994; Beck et al., 1998; Pfiffner, 2014). While valuable as brackets of deformation timing, the existing relative age constraints have several limitations: 1) They only provide maximal and minimal age constraints and do not allow for differentiation between individual tectonic events. 2) It is not unequivocally clear to what extent the maximal age constraints from the distal foreland are representative for faulting along the actual basal décollement underneath the Molasse Basin where the foreland decoupling occurred. 3) Interpretations based on the youngest deformed Tertiary deposits are hampered by the fact that these have been affected by erosion (e.g. Cederbom et al., 2004; Mazurek et al., 2006) causing potential overestimation of the maximal deformation ages.

Previous estimations of the ambient temperatures during deformation along the basal décollement depend mainly on assumptions on the thickness of the Mesozoic and Tertiary sedimentary overburden as well as on the geothermal gradient. Accordingly, temperatures during deformation along the evaporitic basal décollement are thought to generally decrease from 200 C in the proximal parts of the Molasse basin close to the Alps to about 40 C in the Jura Mountains (Sommaruga et al., 2017). Recently, temperatures between 10 and 54 C were reconstructed for fluids associated with the Fuans thrust located in the Late Jurassic limestones of the Internal Jura of eastern France using clumped isotopes (Smeraglia et al., 2020). These temperature data, however were obtained from samples in surface outcrops more than 1 km above the basal décollement and as such do not record ambient temperatures at the décollement.

Our combined clumped isotope and U-Pb data provide the first absolute deformation ages and reconstructions of the temperatures and fluid sources under which the deformation along the basal décollement of the northern Alpine foreland took place. Beyond that, this case-study of the

Jura Mountains illustrates the potential of this conceptual and methodological approach for unravelling multi-phase tectonic histories of orogenic forelands in general.

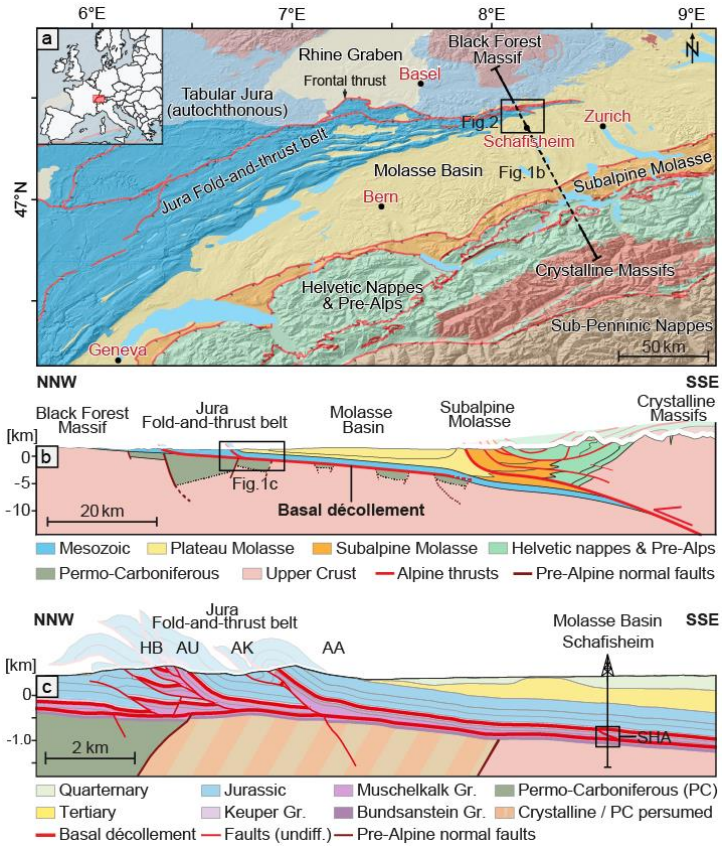

Fig. 1a) Simplified tectonic map of the Central European Alps and their north-western foreland. Fig. 1b) Regional transect with the basal décollement of the Alpine foreland linking the Alps with the Jura fold-and-thrust belt. Figs. 1a and 1b modified after Pfiffner (2014). Fig. 1c) Close-up section across the Schafisheim (SHA) borehole in the distal northern part of the Molasse Basin just south of the Jura range (HB: Habsburg, AU: Asp-Ueslimatt, AK: Asperchlus, AA: Aaretal-Auenstein). Abbreviations indicate the approximate locations of the studied faults. Fig. 1c modified after Jordan et al. (2015).

2 Conceptional approach

Vein cements within the evaporitic décollement are typically composed of anhydrite and are not accessible for U-Pb geochronology and clumped isotope thermometry. We overcome this problem, by analyzing calcite veins associated with thrust faults located between the two main levels of the basal décollement. These thrusts all formed in kinematic relation to deformation along the basal décollement due to Alpine shortening. As they have identical stratigraphic positions close to the main thrust horizon above the mechanical basement, the sampled vein calcites reflect both timing and burial conditions during tectonic activity along the basal décollement. The investigated thrusts are located in two tectonic domains; the distal Molasse Basin and the Jura Mountains (Figs. 1 and 2). Although the thrusts in the two realms cannot

directly be related to each other as they do not share the same tectonic context (see also section 3) they allow to compare the timing as well as the burial conditions during deformation along a N-S transect across the two tectonic domains. For accessing the basal décollement within the Molasse Basin at great depth, we take advantage of the unique sampling opportunity from drill cores of a deep exploration borehole (Schafisheim well, Fig. 1c). In addition to the thrusts, we sampled typical outcrop-scaled strike-slip faults located in the Middle Jurassic of the adjacent Jura Mountains which allows for a comparison between the timing of thrusting and strike-slip faulting in the Jura fold-and-thrust belt.

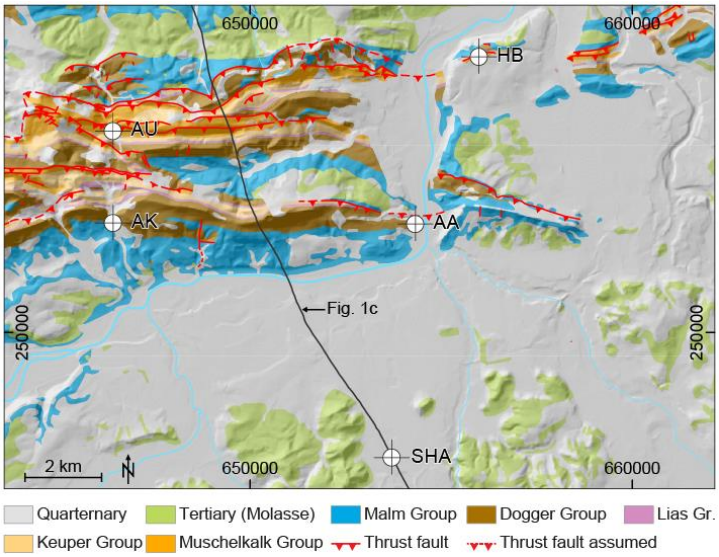

Fig. 2) Detailed geological map of the study area with the locations of the studied thrusts and strike-slip faults. The black line indicates the close-up section of Fig. 1c. Coordinates are given in Swiss Coordinates CH1903.

3 Tectonic sample context

3.1 Schafisheim thrust

The Schafisheim borehole (WGS 84: 47.36950 °N, 8.14855 °E; Matter et al., 1988) is located ~5 km south of the Jura Mountains and ~45 km north of the topographic break related to the frontal thrust of the Subalpine Molasse (Fig. 1). Drill cores were retrieved from most of the basal décollement and structurally analyzed in detail (e.g. Matter et al., 1988; Jordan and Nüesch, 1989). Accordingly, the evaporites of the Triassic Keuper and Muschelkalk groups are the main constituents of the basal décollement at this location and a strongly tectonized salt and anhydrite sequence (1393.35–1435.43 m; Fig. 3a) forms the main thrust horizon above the mechanical basement. A thrust fault (herein called SHA thrust) is located between the two major evaporitic deformation levels and juxtaposes rheologically weak anhydrite-bearing dolostones and marls of the basal décollement on top of rigid limestones. This is evident by a repeated succession within the Muschelkalk Group (lithological units I-III in the footwall and I'-III' in the hanging wall; Fig. 3a; simplified after Matter et al., 1988) and also based on seismic reflection data was recognized as splay structure of the underlying evaporitic basal décollement (Jordan et

al., 2015). The core of this thrust fault (1320.15–1324.70 m) consists of a brecciated dolostone in a claystone-anhydrite matrix and is strongly sheared along sub-horizontal fault planes. In the underlying footwall of the thrust, an approximately 10 m thick damage zone of deformed limestones (Fig. 3b; lithological unit III at 1324.70–1335.26 m) is developed. The uppermost two meters (1324.70–1326.81 m) of this damage zone constitute a cataclastic fault breccia with rotated limestone fragments, sometimes showing sub-vertically oriented sedimentary bedding planes in the otherwise sub-horizontally layered sequence (Figs. 3b and 5b). In the underlying outer damage zone, the sedimentary fabric is intact. A dense network of calcite veins pervades both the cataclastic fault breccia and the outer damage zone of the thrust's footwall from which samples were collected.

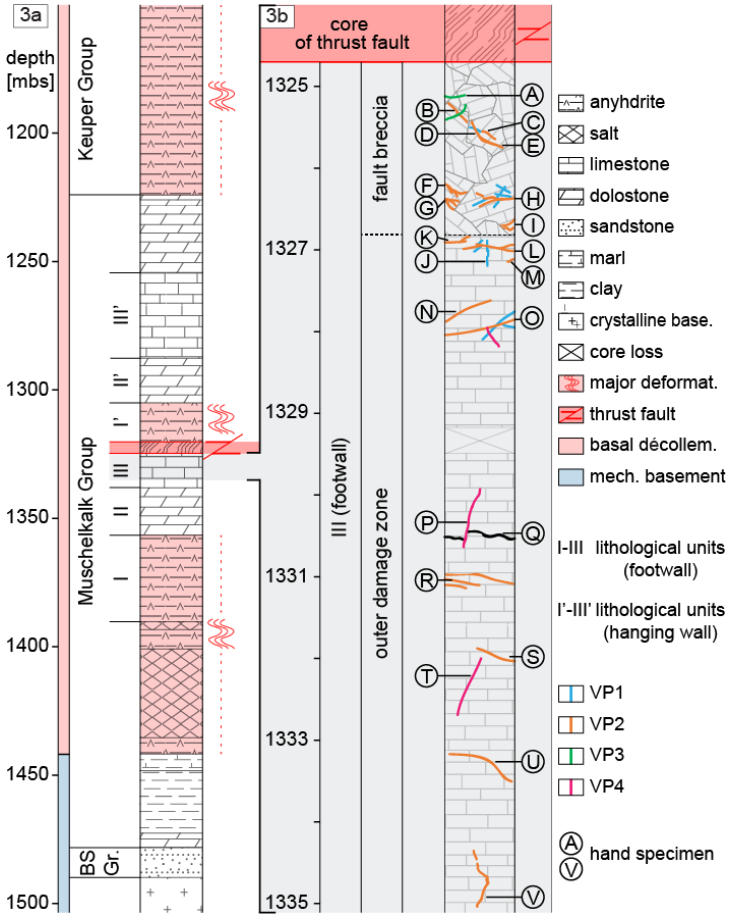

Fig. 3a) Section through the Middle Triassic succession at Schafisheim with the SHA thrust located between the two evaporitic main levels of the basal décollement resulting in a repeated succession (lithological units I-III and I'-III' in the foot and hanging wall, respectively). Fig. 3b) Close-up sketch of the SHA thrust with the sampled veins (simplified). Capital letters refer to hand specimens (A-V) containing analyzed veins (e.g. B-a and B-b; see Fig. 5 and Supplementary Material). Attributed colors indicate vein populations (VP1 veins in blue, VP2 in orange, VP3 in green, and VP4 in pink, see section 5.1).

3.2 Thrusts and strike-slip faults in the eastern Jura Mountains

The eastern Jura Mountains are marked by closely spaced thrust faults along which the basal décollement crops out at the surface. The Mesozoic sedimentary succession exposed in the hanging wall of the thrusts generally dips gently to south (Malz et al., 2016). We collected samples from four locations: Slickenfibers from gently dipping thrust faults within the upper Muschelkalk Group (Schinznach Formation, Middle Triassic) at the locations Habsburg (HB; 47.46305 °N, 8.18160 °E; Figs. 4a, 4b) and Asp-Ueslimatt (AU; 47.44605 °N, 8.05435 °E; Fig. 4c) and slickenfibers from two sub-vertical strike-slip faults within the Dogger Group (Hauptrogenstein Formation, Middle Jurassic) at the locations Aaretal-Auenstein (AA; 47.42466 °N, 8.15890 °E; Fig. 4d) and Asperchlus (AK; 47.42525 °N, 8.05430 °E; Figs. 4e, 4f). The sampled HB and AU thrusts dip gently to the south, almost parallel to the bedding (Figs. 4a and 4c). While a direct connection of these thrust to the basal décollement (such as is clear at the SHA thrust) is not evident, their relation to deformation along it is given due to their kinematic compatibility with NNW-SSE shortening which prevailed during the main phase of Jura thrusting in this area (Becker, 2000; Madritsch, 2015). The sampled AA and AK strike-slip faults (Fig. 2) are typical for the eastern Jura Mountains (Madritsch, 2015) and constrain NNW-SSE shortening in relation to the formation of the Jura fold-and-thrust belt (Madritsch, 2015). Both cut sub-vertically through Middle Jurassic limestones and strike roughly N-S (Figs. 4d and 4e). The centimeter thick slickenfibers on these fault planes indicate sinistral movement (Fig. 4f), also being compatible with Miocene NNW-SSE shortening (Becker, 2000; Madritsch, 2015). Notably, the strike-slip slickenfibers are oriented parallel to the bedding and dip gently to the south. This was previously interpreted as tilting due to thrust-related folding post-dating calcite precipitation and strike-slip faulting (Madritsch, 2015).

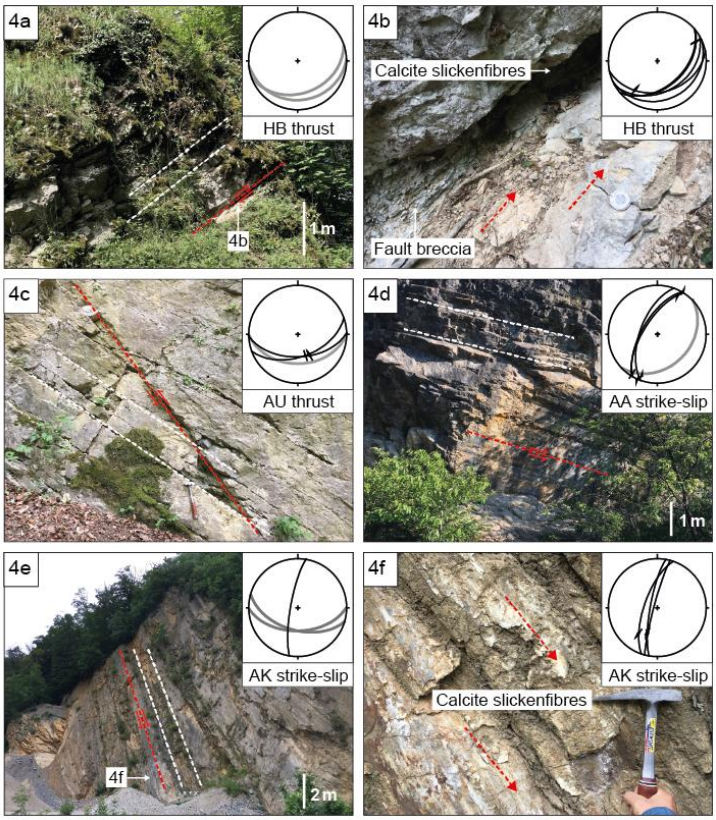

Fig. 4a-4f) Field impressions of the sampled thrusts and strike slip faults in the eastern Jura Mountains (see Fig. 2 for locations). The white lines indicate the bedding orientations. The red lines indicate the sampled faults (Figs. 4a and 4c) or fault-slip lineation (Figs. 4b, 4d, 4e, and 4f). Inserted stereo plots are lower hemisphere, equal area projections showing bedding orientation and fault orientation in grey and black, respectively.

4 Analytical methods

4.1 Calcite U-Pb LA-ICP-MS dating

Calcite U-Pb dating was performed by laser ablation inductively coupled plasma mass spectrometry (LA-ICP-MS) on polished thick sections and chips mounted in epoxy at ETH Zurich using an ASI RESOlution S-155, excimer (ArF, 193 nm) laser ablation system coupled to a Thermo Element XR sector-field ICP-MS. The analytical method and correction procedure follow Roberts et al. (2017) using NIST 614 and WC-1 primary reference materials and (Guillong et al., 2020). U-Pb ages were calculated from Tera-Wasserburg concordia lower intercepts using the IsoplotR software package (Vermeesch, 2018). All uncertainties are reported at 95% confidence level. A long-term excess variance of 2.5% relative was propagated by quadratic addition to the uncertainty of the individual, lower intercept dates (Guillong et al., 2020). Prior to and after LA-ICP-MS measurements, cathodoluminescence microscopy was conducted in order to identify growth zonings and to identify misplaced ablation spots which then were excluded from the data. In addition to this, the lower intercept dates showing a MSWD value > 4.3 or an uncertainty > 2 Ma were not considered.

4.2 Clumped isotope thermometry

Clumped isotope analyses were conducted at ETH Zurich using a Thermo Scientific Kiel IV carbonate device coupled to a Thermo Scientific MAT253 isotope ratio mass spectrometer (IRMS) based on the methods described by Müller et al. (2017). Mineralogy was checked by XRD prior to analysis to avoid carbonate mixtures. In addition to the removal of water and non-condensable gases by the Kiel IV carbonate device, potential isobaric contaminations were removed by a Porapak Q resin held at -40 °C. Backgrounds on m/z 44 to 47 were determined at the beginning of each analytical session by high-voltage peak scans at 5 different intensities between 10 and 30 V. Data reduction was carried out with the Easotope software package (John and Bowen, 2016). Normalization and projection of clumped isotope measurements into the carbon dioxide equilibrium scale (CDES) was done using the carbonate standards ETH-1, ETH-2, and ETH-3 with the values of (Bernasconi et al., 2018). Δ_{47} temperatures were calculated with the recalculated Kele et al. (2015) calibration (Bernasconi et al., 2018) and $\delta^{18}O_{fluid}$ was calculated using the calibration of (Kim and O'Neil, 1997). Measurements with a deviation from the median Δ_{47} value $\geq$ 0.090‰ (2% of all measurements) were not considered.

5 Results

5.1 Structural analysis

At the SHA thrust, secondary calcites in veins pervading the cataclastic fault breccia and the outer damage zone of the thrust's footwall (Fig. 3) show syntaxial, elongated blocky and blocky textures. Based on structural observations (crosscutting relationships and vein orientations), we initially differentiated between four populations of calcite veins in the footwall of the SHA thrust (VP1-VP4, from old to young; Figs. 3b and 5). Veins of VP1 (blue) are thin and crosscut by VP2 veins (orange) while exhibiting various dips. Veins of VP2 in the outer damage zone mostly show sub-horizontal orientations. Within the fault breccia, VP2 veins are often tectonized themselves (truncated at clast boundaries; Figs. 5b and 5e) and structurally pre-date the thrust-related cataclasis. In the outer damage zone, these veins are occasionally associated with dip-slip slickenfibers indicating thrust kinematics. Veins of VP3 (green) are found exclusively within the fault breccia and differ from VP2 in overprinting the cataclastic fabric by cutting through multiple clasts. Thus, they formed syn- or post-cataclasis. Veins of VP4 (pink) show sub-vertical orientations and cut through veins of VP1 to VP3. Given the fact that the Schafisheim cores are non-oriented, the azimuth of these veins remains unknown.

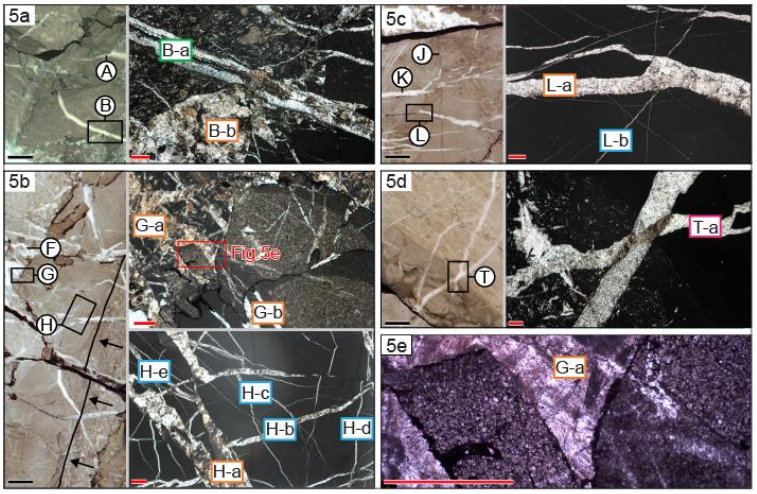

Figs. 5a- 5d show core photographs with black squares indicating the location of thin-section images on the right. Scale bars indicate 20 mm (black) and 2 mm (red). Fig. 5a) VP3 veins (A, B-a) overprint the cataclastic texture of the fault breccia by cutting through multiple clasts and a VP2 vein (B-b). Fig. 5b) Fault breccia with rotated clasts indicated by a sub-vertical sedimentary bedding plane (black line marked by arrows). The magnified sections show the cataclastic overprint of VP2 veins (G-a and G-b) being truncated at clast boundaries and VP1 veins being crosscut by VP2 veins (e.g. H-a vs. H-b and H-e). Fig. 5c) VP2 veins in the outer damage zone with the original sub-horizontal orientation and a VP1 vein (L-b) being crosscut by a VP2 vein (L-a). Fig. 5d) Sub-vertical VP4 vein crosscutting an earlier vein of unknown age. Fig. 5e shows the truncation of a VP2 vein at a clast boundary (G-a, indicated by a red square in Fig. 5b) under an optical microscope. The scale bar indicates 2 mm.

5.2 Calcite U-Pb LA-ICP-MS analysis

A total of 45 vein calcites yielded reliable age data. A selection of Tera-Wasserburg concordia diagrams of a representative subset of samples covering all observed deformation intervals are shown in Fig. 6 and the complete set of Tera-Wasserburg plots can be found as Supplementary Material.

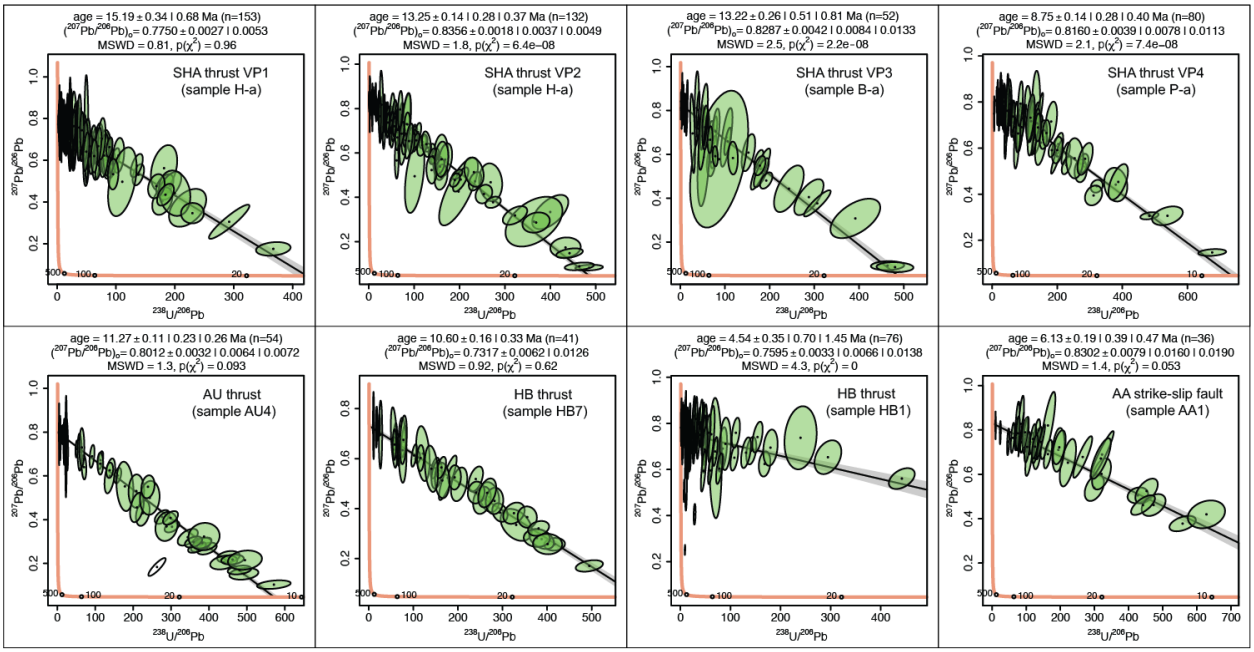

Fig. 6) Tera-Wasserburg concordia diagrams of a representative subset of samples (created with the IsoplotR software package; Vermeesch, 2018).

For the SHA thrust, the age of each vein population and its uncertainty were determined by calculating a weighted mean based on all individual vein lower intercept ages of the population. This is justified by the fact that the vein populations are structurally constrained to correspond to different deformation phases. VP1 yielded a resulting weighted mean age of 14.3 ± 0.5 Ma (n = 9). The weighted means of lower intercept ages for VP2 and VP3 are indistinguishable from each other, with a mean age of 13.2 ± 0.2 Ma obtained when pooled together (VP2 & VP3, n = 21). VP4 shows a weighted mean age of 9.1 ± 1.4 Ma (n = 3). We note that, although some of the individual vein ages of the two populations overlap within uncertainties, the offset between the average ages of VP1 and VP2 & VP3 is statistically significant, by minimum 0.5 Ma and maximum 1.7 Ma when considering uncertainties at the 95% confidence level (CL).

For the outcrops in the eastern Jura Mountains, the reported U-Pb ages correspond to single dates of individual samples. Because of the limited number of samples and the large spread of ages, no weighted means were calculated. The slickenfibers from the AU thrust yielded four U-Pb ages between 11.3 ± 0.9 Ma and 9.9 ± 0.6 Ma. The slickenfibers from the HB thrust plot in two groups with significantly different ages: A first group with four ages ranging from 10.6 ± 0.4 Ma to 8.1 ± 0.6 Ma and a second group with two ages of 5.7 ± 0.7 Ma and 4.5 ± 1.5 Ma, respectively. The sample from the AK strike-slip fault yielded a lower intercept age of 9.3 ± 1.1 Ma and the sample from the AA strike-slip fault of 6.1 ± 0.5 Ma, respectively. The age data of the AK strike-slip fault is in good agreement with the only other reported calcite slickenfiber U-Pb age of 9.05 ± 0.94 Ma, stemming from a similar structural feature in the Jura Mountains approx. 25 km west of Schafisheim (Rittner, 2013; Madritsch, 2015).

306 5.3 Clumped isotope analysis

307 A total of 306 measurements of 25 samples were considered for the reconstruction of
308 formation temperatures and the composition of the precipitating fluids. Errors in Δ_{47}
309 temperatures are reported at the 95% confidence level (Fernandez et al., 2017). A table with all
310 data can be found as Supplementary Material and the whole data set including the carbonate
311 standards is available as Easotope Database upon request. When plotted as Δ_{47} temperature vs.
312 $\delta^{18}O_{fluid}$, the data from the different sites and fault types group in fields reflecting three distinct
313 burial settings at the time of faulting (Fig. 7).

314

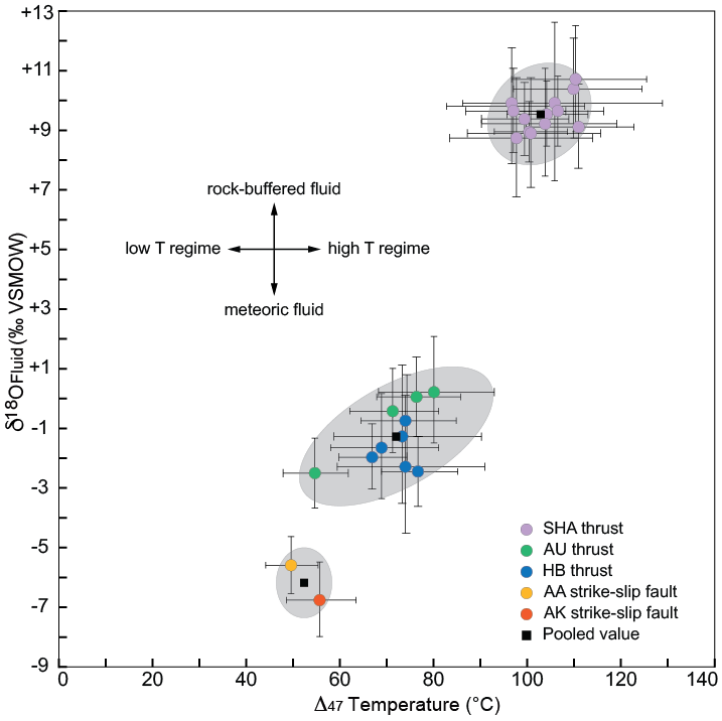

315

316 Fig. 7) Clumped isotope data plotted as Δ_{47} temperature vs. $\delta^{18}O_{fluid}$ with the error bars showing
317 95% confidence intervals (see text for discussion).

318

319 For the SHA thrust, clumped isotope (Δ_{47}) temperatures and calculated oxygen isotope
320 compositions of the precipitating fluid ($\delta^{18}O_{fluid}$) of the four vein populations are
321 indistinguishable from each other at the 95% CL (Fig. 7) and pooled together yielded a Δ_{47}
322 temperature of 104 ± 3 °C and a $\delta^{18}O_{fluid}$ of +9.5 ± 0.4 ‰, VSMOW. The samples from the AU
323 and HB thrusts overlap in most cases in both Δ_{47} temperatures and $\delta^{18}O_{fluid}$ at the 95% CL
324 (Fig. 7) and therefore were also pooled together (AU & HB) yielding a Δ_{47} temperature of 73 ±
325 3 °C and a $\delta^{18}O_{fluid}$ of -1.3 ± 0.5 ‰, VSMOW. The same procedure was applied for the AK and
326 AA strike-slip faults (AK & AA) yielding a pooled Δ_{47} temperature of 53 ± 4 °C and a $\delta^{18}O_{fluid}$
327 of -6.2 ± 0.8 ‰, VSMOW.

328

6 Discussion

6.1 Timing of deformation

Figure 8 shows a compilation and interpretation of the U-Pb data from the SHA thrust. The oldest recorded deformation ages related to tectonic activity of the basal décollement at this location occurred during a time interval between ~14.5 and ~12.5 Ma. There, VP1 dated at 14.3 ± 0.5 Ma on average is the earliest evidence for brittle deformation in the thrust's footwall. Besides being overprinted by cataclasis related to thrusting, a direct kinematic relation of VP1 to the thrust is not well constrained but is most likely for two reasons. First, VP1 veins are restricted to the damage zone in the footwall of the thrust. Second, clumped isotopes show that they formed under very similar temperature conditions to the other populations with well-established structural relations to the thrust. Therefore, we infer VP1 to be related to Alpine shortening, representing the minimum age for its onset. Unambiguous evidence for a phase of thrusting at Schafisheim at 13.2 ± 0.2 Ma is provided by VP2 & VP3. The fact that VP2 and VP3 yield identical U-Pb ages while showing different structural relationships (VP2 being overprinted by the cataclastic fabric and VP3 overprinting the same) gives excellent constraints on the timing of cataclasis in the thrust's footwall (Fig. 8).

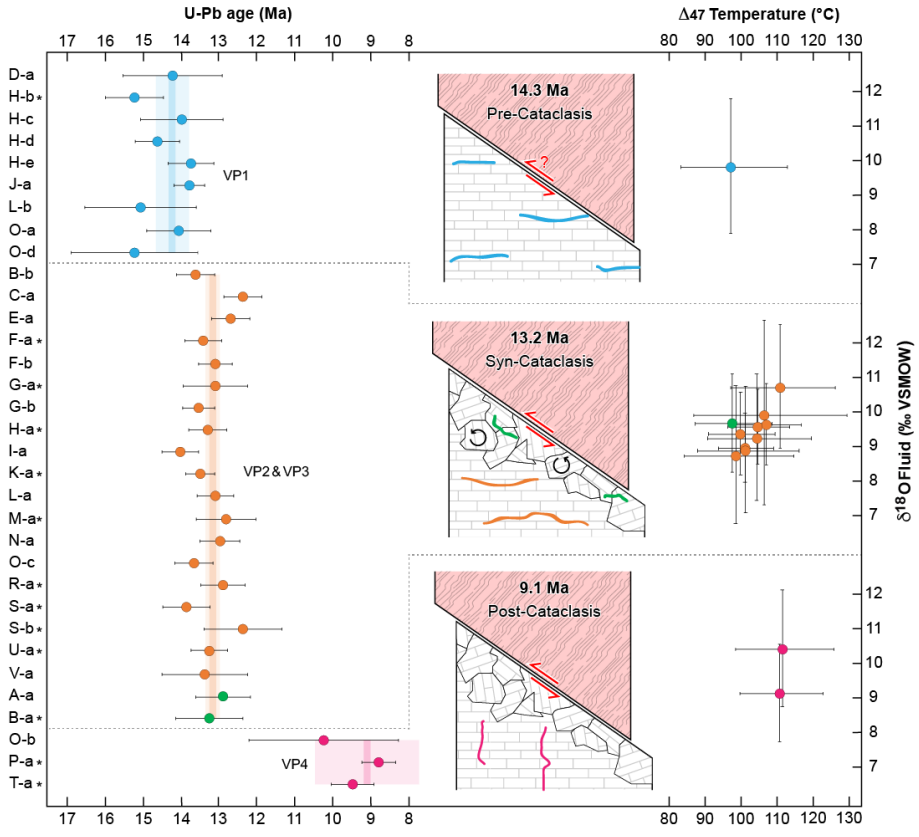

Fig. 8) Reconstruction of the SHA thrust evolution and related vein formation with U-Pb and clumped isotope data. Colors correspond to vein populations (VP1 in blue, VP2 in orange, VP3 in green, and VP4 in pink) as in Figs. 3b and 5. Letters on the left side refer to the veins as in Fig. 5 and in the Tera-Wasserburg isochron diagrams and sample images in the Supplementary

Material. Veins analyzed for clumped isotopes are indicated with stars. Error bars show 95% CLs for both clumped isotope and individual U-Pb data of calcite veins. Dark shaded lines show the weighted mean U-Pb age and the lighter shading the uncertainty at the 95% CL for each vein population.

Figure 9 shows a compilation of the U-Pb data from all sample locations and fault types (Fig. 2). Evidently, the thrusts and strike-slip faults from the eastern Jura Mountains constrain younger phases of foreland deformation between ~11.5 and ~4.5 Ma implying a duration of thrusting activity of at least about 10 Ma (14.3 to 4.5 Ma). While the youngest recorded deformation at Schafisheim is at ~9 Ma, deformation records in the adjacent Jura Mountains are as young as 4.5 Ma. Notably, thrusting occurred simultaneously with strike-slip faulting. Since the strike-slip faults were already active prior to large-scale thrust-related folding (Madritsch, 2015), this process occurred in a late tectonic stage (post 9 Ma, based on the AK strike-slip fault).

The observed time lag of 3 Ma between the reconstructed onsets of deformation at the SHA thrust (14.3 Ma) and in the Jura Mountains (11.3 Ma) implies a foreland-directed thrust propagation signal (Fig. 9). However, the U-Pb data needs to be interpreted with caution in this regard because of the spatially limited coverage of the available samples. In other words, potential older deformation in other locations in the Jura Mountains than at the studied faults may have simply been missed. Similarly, we must regard the oldest ages form the SHA thrust as a minimum age for the onset of tectonic activity along the basal décollement and consider that deformation initiated even earlier.

Our data from the Schafisheim well constrains earlier thrusting along the basal décollement than commonly inferred for the Jura Mountains (late Serravallian or later; Sommaruga et al., 1995; Kälin, 1997; Becker, 2000; Ziegler and Fraefel, 2009; Rittner, 2013; Madritsch, 2015; Malz et al., 2016) already starting in Langhian times at the latest. This corroborates isolated field observations of early-stage foreland shortening close to the Alpine front already during Burdigalian times (Deville et al., 1994; Beck et al., 1998; Pfiffner, 2014). Combining our data with the existing biostratigraphic age constraints from different locations in the foreland suggests the initiation of decoupling and thrusting along the basal décollement at ~20-16 Ma close to the Alpine front (Deville et al., 1994; Beck et al., 1998; Pfiffner, 2014), followed by foreland-directed propagation of deformation towards the distal Molasse Basin at Schafisheim (14.3 Ma, this study), to the Internal Jura Mountains at 11.5 Ma (this study), and finally to the frontal thrusts at ~11-9 Ma (Kälin, 1997, Becker, 2000 and references therein).

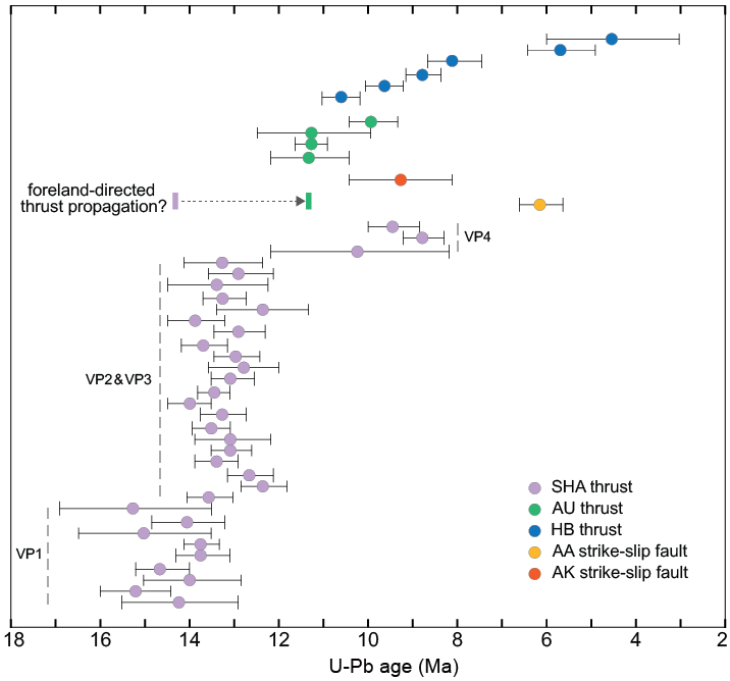

Fig. 9) U-Pb data from the different sites arranged as a S-N transect. Error bars show 95% confidence intervals.

The indications for early-stage thrusting at Schafisheim predate thermochronologically constrained thrust pulses between 12 and 5 Ma in the Subalpine Molasse of the more proximal foreland (Figs. 1a and 1b; von Hagke et al., 2012; Mock et al., 2019). This may imply an initial backward breaking sequence of foreland thrusting across the north-western Alpine foreland as similarly suggested for the Subalpine Molasse further to the east (Ortner et al., 2015). However, the same authors mention that stratigraphic data suggests tectonic activity in this region before 12 Ma. The younger pulses of deformation between ~11.5 and ~4.5 Ma in our area of investigation corresponds very well with evidences for shortening in the Subalpine Molasse and also the Central Alps (von Hagke et al., 2012; Herwegh et al., 2019). This proves simultaneous tectonic activity along both thrust fronts; e.g. the Jura Mountains and the Subalpine Molasse over a time span of several million years as suggested by von Hagke et al. (2012).

6.2 Temperatures and fluid flow during deformation

Figure 10 shows the clumped isotope data plotted against the corresponding U-Pb ages measured on the same samples. Contemporaneous deformation recorded at the different sites during the time interval at ~11.5-8 Ma allows for a direct comparison of the deformation temperatures and syntectonic fluid flow between the different burial settings (the distal Molasse Basin vs. the Jura Mountains) and fault types (thrusts vs. strike-slip faults). At the SHA thrust, the pooled $\delta^{18}O_{fluid}$ of +9.5 ± 0.4 ‰ (VSMOW) indicate precipitation from a parent fluid modified by extensive fluid-rock interaction at high temperatures. Equilibration of a fluid with the host rock, for which we measured a $\delta^{18}O$ of -5.94 ‰ (VPDB), at 104 °C will result in a $\delta^{18}O_{fluid}$ of +9.1 ‰ (VSMOW). The consistency of the recorded $\delta^{18}O_{fluid}$ with the expected

values for equilibrium shows that the vein calcites at the SHA thrust precipitated from a fluid in or near equilibrium with the host rock. Therefore, the vein calcites reflect ambient burial temperatures during times of faulting. Because of the equilibration of the oxygen isotope composition with the host rock, the calculated $\delta^{18}O_{fluid}$ does not indicate its origin. Thus, it remains open if the fluid sourced from greater depth and migrated upwards along the thrust fault or if it originally was of meteoric origin and infiltrated from the overlaying units. In either case, the flow rate was low enough for thermal and oxygen isotopic equilibration with the host rock.

Compared to the SHA thrust, the AU and HB thrusts with a pooled Δ_{47} temperature of 73 ± 3 °C and a pooled $\delta^{18}O_{fluid}$ of -1.3 ± 0.5 ‰ (VSMOW) imply significantly less overburden at the time of faulting in the Jura Mountains. This difference is interpreted to reflect the northward decreasing thickness of Molasse deposits. A fluid in equilibrium with the host rock at the AU and HB thrusts with a $\delta^{18}O$ of -5.62 ‰ and a temperature of 73 °C would have a $\delta^{18}O_{fluid}$ of +5.2 ‰ (VSMOW), much more enriched in ^{18}O than the -1.3 ‰ observed. There are two scenarios that can explain this observation. Based on our data, both scenarios are possible and for both cases, we argue that the 73 °C recorded by the slickenfiber calcites approximate the ambient temperatures during times of faulting at the AU and HB thrusts. In the first scenario, meteoric fluids infiltrated from the overlaying units and in absence of other fluids were heated up while only partially equilibrating in oxygen isotopes with the host rock and maintaining some of the original isotopically light meteoric signatures. This scenario implies that these thrusts were connected to the surface or shallow groundwater aquifers. As thermal equilibration takes place much faster than oxygen isotope exchange, a fluid with a substantial modification of is original oxygen isotope composition due to water-rock interaction will reach the same temperature as the host rock. In the second scenario, deep-seated hot fluids rapidly ascended along the fault zone, for example during earthquakes, and mixed with colder pore waters, as was shown in an active fault in the Appennines (Smeraglia et al., 2018). This scenario is consistent with evidence for fluid flow along the crystalline basement and/or the lowermost sedimentary unit, the Bundsandstein Group (Fig. 3), sourcing from infiltration of meteoric waters in the Black Forest highland (Fig. 1) and ascending into the lower Mesozoic formations along cross-formational faults in the northeastern Swiss Molasse Basin (Aschwanden et al., 2019). As the difference in burial between the basal décollement and the crystalline basement is only minor (e.g. some more than 50 m at Schafisheim, see Fig. 3) and since fluid flow most likely was concentrated in the permeable weathering zone of the basement and/or the lowermost sedimentary unit, the ascending fluids were only few degrees warmer than ambient burial temperatures at the basal décollement. Moreover, the local extent of the AU and HB thrusts with no large-scale network of veins speak against a rapid fluid ascend so that, if sourcing from greater depth, the ascending fluids would have thermally equilibrated with the host rock.

A maximum value for the $\delta^{18}O$ of the unmodified meteoric endmember (e.g. before interaction with the host rocks during infiltration) is provided by the AA and AK strike-slip faults showing the most depleted observed oxygen isotope signatures of -6.2 ± 0.8 ‰ (VSMOW) when pooled together. Compared to this value, the reconstructed fluids from the AU and HB thrusts are about 5 ‰ enriched. During the time needed for this enrichment, temperatures will have fully equilibrated. Accordingly, we consider the Δ_{47} temperatures from the AU and HB thrusts as close approximation for the ambient temperatures during deformation at the basal décollement in the region of the present-day eastern Jura Mountains. The AA and AK strike-slip faults show a colder pooled Δ_{47} temperature of 53 ± 4 °C and much more meteoric $\delta^{18}O_{fluid}$

signatures compared to the AU and HB thrusts. To some extent, this may be due to the location of these faults, approximately 400 m higher in the stratigraphic column (Middle Jurassic Hauptrogenstein Fm. vs. Middle Triassic Schinznach Fm.). Furthermore, the steepness of the strike-slip faults has likely favored meteoric water infiltration at higher rates resulting in less water-rock interaction. Therefore, the 53 ± 4 °C recorded by the slickenfibers could be lower than the ambient burial temperatures.

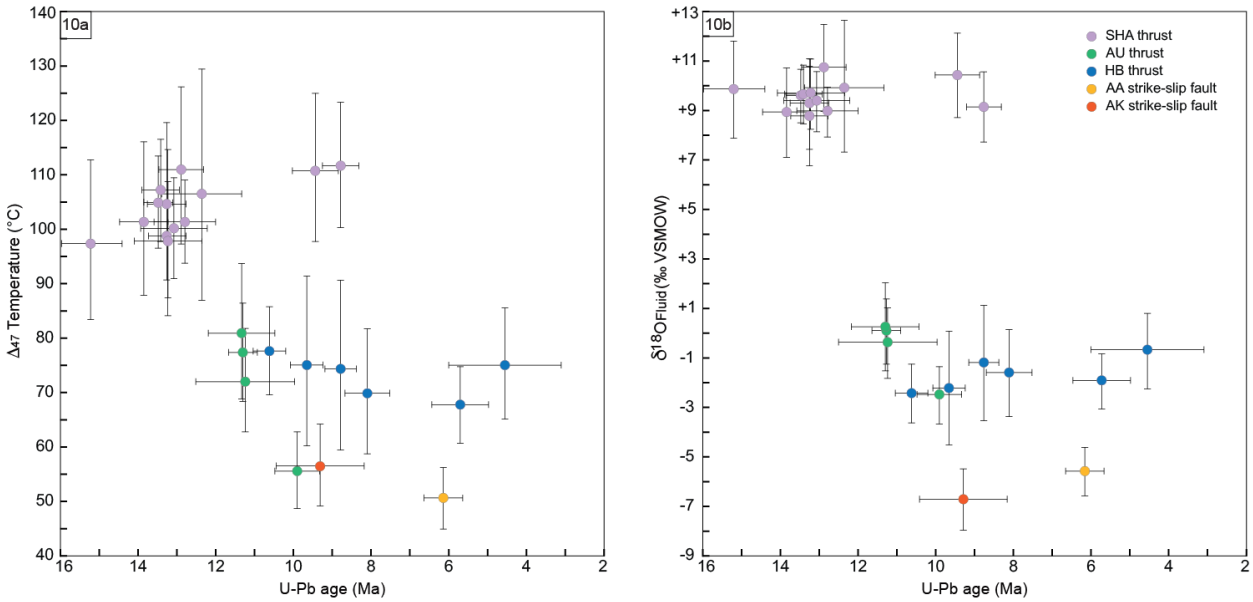

Fig. 10) Δ_{47} temperatures (Fig. 10a) and $\delta^{18}O_{fluid}$ (Fig. 10b) of the vein calcites plotted against their corresponding U-Pb ages.

Since the SHA thrust as well as the AU and HB thrusts are located close to the basal décollement and underwent thermal equilibration with the host rocks, the Δ_{47} temperatures of the veins constrain deformation within the décollement during basal thrusting. The temperature difference of 30 °C between the interior of the distal Molasse Basin and the present-day Jura Mountains along the basal décollement correlates with distinct microfabrics of anhydrite mylonites defining deformation regimes of temperature and deformation mechanisms (Jordan, 1992). Thermal equilibrium at the SHA, HB, and AU thrusts allows for estimations of deformation depths. Assuming a geothermal gradient between 20 °C km^{-1} (Mazurek et al., 2006) and 30 °C km^{-1} (Cederbom et al., 2004) and a temperature of the infiltrating meteoric fluids of 10 °C (modern temperature of springs in the Jura Mountains, Jeannin et al., 2016), thrusting took place under 3.1-4.7 km of sedimentary overburden at Schafisheim and under 2.1-3.1 km in the eastern Jura mountains, respectively.

Widely constant Δ_{47} temperatures and $\delta^{18}O_{fluid}$ over time implies deformation under constant burial conditions (Figs. 10a and 10b). Accordingly, the faults did not experience significant exhumation either through piggy-back transport along the shallow dipping décollement or erosion of the overlaying sediments or further burial between 14.3 and 4.5 Ma. This confirms apatite fission track data suggesting inversion and initiation of major erosion in the

485 northwestern Alpine foreland at ~5 Ma (Kuhlemann and Kempf, 2002; Cederbom et al., 2004,
486 2011).

487 Based on the calculated sedimentary overburden during thrusting, we estimate 2.0-3.6 km
488 of erosion at Schafisheim since Pliocene times. This value overlaps with other estimates for
489 erosion of the undeformed Molasse in Switzerland of 1 km (Mazurek et al., 2006; assumed
490 goethermal gradient of $\leq$20 °C km^{-1}), 2-2.6 km (Schegg et al., 1997; assumed geothermal
491 gradient of 30 °C km^{-1}), 1.4-3.5 km (Cederbom et al., 2004; assumed geothermal gradient of 20-
492 30 °C km^{-1}) and 0.7-2.7 km (Cederbom et al., 2011; assumed goetheral gradient of 25-37 °C km^{-}
493 ^{1}) based on vitrinite reflectance and apatite fission tracks data.

494

495 **7 Conclusion**

496 The combined carbonate U-Pb and clumped isotope data presented here provide the first
497 absolute age and temperature constraints for deformation along the basal décollement of the Jura
498 Mountains, a classical example for a thin-skinned foreland fold-and-thrust belt and allows to
499 draw four major conclusions. 1) The age data from the distal Molasse Basin at Schafisheim
500 shows that thrusting along the basal décollement was active earlier than commonly inferred for
501 the Jura Mountains, already at Langhian times. 2) The associated deformation was not a short-
502 lived event but occurred over a time period between at least 14.3 and 4.5 Ma with
503 contemporaneous activity (and potential interplay) of thrusts and strike-slip faults in the Jura
504 Mountains. 3) Over this time period, the burial conditions remained constant showing that large-
505 scale erosion of the Molasse Basin at its northern margin took place after ~4.5 Ma. 4) The
506 reconstructed temperatures and fluid compositions show an increase in burial of the basal
507 décollement from north to south, reflecting different amounts of Molasse overburden and
508 provide constraints for in-situ temperatures during deformation and syntectonic fluid flow.
509 Beyond that, our study demonstrates the great potential of combined carbonate U-Pb
510 geochronology and clumped isotope thermometry for reconstructing the absolute timing as well
511 as the temperatures and fluids involved in foreland thrust systems and provides perspectives for
512 further studies.

513

514 **Acknowledgments, Samples, and Data**

515 We thank the Swiss National Cooperative for the Disposal of Radioactive Waste (Nagra)
516 for access to the Schafisheim cores. This study was funded by the Swiss National Science
517 Foundation project number 200021_169849. Data archiving complying with FAIR Data
518 guidelines is underway and a copy of the data sets is submitted toghether with the manuscript as
519 supporting information for review purposes. The entire U-Pb and clumped isotope data sets
520 aswell as sample pictures will be available to the public at the data sharing infrastructures of
521 Geochron (https://www.geochron.org) and EarthChem (http://earthchem.org), respectively.

522

References

Aschwanden, L., Diamond, L.W., Mazurek, M., and Davis, D.W., 2019, Creation of Secondary Porosity in Dolostones by Upwelling Basement Water in the Foreland of the Alpine Orogen, Geofluids, v. 2019, doi:10.1155/2019/5210404.

Beaudoin, N., Lacombe, O., Roberts, N.M.W., and Koehn, D., 2018, U-Pb dating of calcite veins reveals complex stress evolution and thrust sequence in the Bighorn Basin, Wyoming, USA: Geology, v. 46, p. 1015–1018, doi:10.1130/G45379.1.

Beck, C., Deville, E., Blanc, E., Philippe, Y., and Tardy, M., 1998, Horizontal shortening control of Middle Miocene marine siliciclastic accumulation (Upper Marine Molasse) in the southern termination of the Savoy Molasse Basin (northwestern Alps/southern Jura): Geological Society Special Publication, v. 134, p. 263–278, doi:10.1144/GSL.SP.1998.134.01.12.

Becker, A., 2000, The Jura Mountains - an active foreland fold-and-thrust belt? Tectonophysics, v. 321, p. 381–406, doi:10.1016/S0040-1951(00)00089-5.

Bernasconi, S.M., Müller, I.A., Bergmann, K.D., Breitenbach, S.F.M., Fernandez, A., Hodell, D.A., Jaggi, M., Meckler, A.N., Millan, I., and Ziegler, M., 2018, Reducing Uncertainties in Carbonate Clumped Isotope Analysis Through Consistent Carbonate-Based Standardization: Geochemistry, Geophysics, Geosystems, v. 19, p. 2895–2914, doi:10.1029/2017GC007385.

Bolliger, T., Engesser, B., and Weidmann, M., 1993, Première découverte de mammifères pliocènes dans le Jura neuchâtelois: Eclogae Geologicae Helvetiae, v. 86, p. 1031–1068.

Burkhard, M., 1990, Aspects of the large-scale Miocene deformation in the most external part of the Swiss Alps (Subalpine Molasse to Jura fold belt): Eclogae Geologicae Helvetiae, v. 83, p. 559–583.

Buxtorf, A., 1907, Zur Tektonik des Kettenjura: Berichte u¨ber die Versammlungen des Oberrheinischen geologischen Vereins, v. 40, p. 79–111.

Cederbom, C.E., Van Der Beek, P., Schlunegger, F., Sinclair, H.D., and Oncken, O., 2011, Rapid extensive erosion of the North Alpine foreland basin at 5-4Ma: Basin Research, v. 23, p. 528–550, doi:10.1111/j.1365-2117.2011.00501.x.

Cederbom, C.E., Sinclair, H.D., Schlunegger, F., and Rahn, M.K., 2004, Climate-induced rebound and exhumation of the European Alps: Geology, v. 32, p. 709–712, doi:10.1130/G20491.1.

Deville, E., Blanc, E., Tardy, M., Beck, C., Cousin, M., and Ménard, G., 1994, Thrust Propagation and Syntectonic Sedimentation in the Savoy Tertiary Molasse Basin (Alpine Foreland): Hydrocarbon and Petroleum Geology of France, p. 269–280, doi:10.1007/978-3-642-78849-9_19.

Fernandez, A., Müller, I.A., Rodríguez-Sanz, L., van Dijk, J., Looser, N., and Bernasconi, S.M., 2017, A Reassessment of the Precision of Carbonate Clumped Isotope Measurements: Implications for Calibrations and Paleoclimate Reconstructions: Geochemistry, Geophysics, Geosystems, v. 18, p. 4375–4386, doi:10.1002/2017GC007106.

Guillong, M., Wotzlaw, J., Looser, N., and Laurent, O., 2020, Evaluating the reliability of U – Pb laser ablation inductively coupled plasma mass spectrometry (LA-ICP-MS) carbonate geochronology : matrix issues and a potential calcite validation reference material: , p. 155–167.

Von Hagke, C., Cederbom, C.E., Oncken, O., Stckli, D.F., Rahn, M.K., and Schlunegger, F., 2012, Linking the northern Alps with their foreland: The latest exhumation history resolved by low-temperature thermochronology: Tectonics, v. 31, p. 1–25, doi:10.1029/2011TC003078.

Herwegh, M., Berger, A., Glotzbach, C., Wangenheim, C., Mock, S., Wehrens, P., Baumberger, R., Egli, D., and Kissling, E., 2019, Late Stages of Continent-Continent Collision: Timing, Kinematic Evolution, and Exhumation of the Northern Rim (Aar Massif) of the Alps: Earth Science Reviews, v. 200, p. 102959, doi:10.1016/j.earscirev.2019.102959.

Huntington, K.W., and Lechler, A.R., 2015, Carbonate clumped isotope thermometry in continental tectonics: Tectonophysics, v. 647, p. 1–20, doi:10.1016/j.tecto.2015.02.019.

Jeannin, P.Y., Hessenauer, M., Malard, A., and Chapuis, V., 2016, Impact of global change on karst groundwater mineralization in the Jura Mountains: Science of the Total Environment, v. 541, p. 1208–1221, doi:10.1016/j.scitotenv.2015.10.008.

John, C.M., and Bowen, D., 2016, Community software for challenging isotope analysis : First applications of ‘ Easotope ’ to clumped isotopes: Rapid Communications in Mass Spectrometry, p. 2285–2300, doi:10.1002/rcm.7720.

Jordan, P., 1992, Evidence for large-scale decoupling in the Triassic evaporites of northern Switzerland: an overview: Eclogae Geologicae Helvetiae, v. 85, p. 677–693.

Jordan, P., Malz, A., Heuberger, S., Pietsch, J., Kley, J., and Madritsch, H., 2015, Regionale geologische Profile durch die Nordschweiz und 2D-Bilanzierung der Fernschubdeformation im östlichen Faltenjura. Nagra Project Report, NAB 14-105, Nagra, Wettingen.:

Jordan, P., and Nüesch, R., 1989, Deformation structures in the Muschelkalk anhydrites of the Schafisheim Well (Jura Overthrust, northern Switzerland): Eclogae Geologicae Helvetiae, v. 82, p. 429–454.

Kälin, D., 1997, Litho- und Biostratigraphie der mittel- bis obermiozänen Bois de Raube-Formation (Nordwestschweiz): Eclogae Geologicae Helvetiae, v. 90, p. 97–114.

Kele, S. et al., 2015, study of travertines and tufas in the 6-95°C temperature range: GEOCHIMICA ET COSMOCHIMICA ACTA, doi:10.1016/j.gca.2015.06.032.

Kim, S.T., and O’Neil, J.R., 1997, Equilibrium and nonequilibrium oxygen isotope effects in synthetic carbonates: Geochimica et Cosmochimica Acta, v. 61, p. 3461–3475, doi:10.1016/S0016-7037(97)00169-5.

Kuhlemann, J., and Kempf, O., 2002, Post-Eocene evolution of the North Alpine Foreland Basin and its response to Alpine tectonics: Sedimentary Geology, v. 152, p. 45–78, doi:10.1016/S0037-0738(01)00285-8.

Laubscher, H.P., 1978, Foreland folding: Tectonophysics, v. 47, p. 325–337, doi:10.1016/0040-1951(78)90037-9.

Madritsch, H., 2015, Outcrop-scale fracture systems in the Alpine foreland of central northern Switzerland: kinematics and tectonic context: Swiss Journal of Geosciences, v. 108, p. 155–181, doi:10.1007/s00015-015-0203-2.

Malz, A., Madritsch, H., Meier, B., and Kley, J., 2016, An unusual triangle zone in the external northern Alpine foreland (Switzerland): Structural inheritance, kinematics and implications for the development of the adjacent Jura fold-and-thrust belt: Tectonophysics, v. 670, p. 127–143, doi:10.1016/j.tecto.2015.12.025.

Mangenot, X., Gasparrini, M., Gerdes, A., Bonifacie, M., and Rouchon, V., 2018, An emerging thermochronometer for carbonate-bearing rocks: Δ47 /(U-Pb): Geology, v. 46, p. 1067–1070, doi:10.1130/G45196.1.

Matter, A., Peters, T., Bläsi, H.-R., Schenker, F., and Weiss, H.-P., 1988, Sondierbohrung Schafisheim – Geologie Textband und Beilagenband. Nagra Technischer Bericht 86-03. Landeshydrologie und -geologie, Bern.

Mazurek, M., Hurford, A.J., and Leu, W., 2006, Unravelling the multi-stage burial history of the Swiss Molasse Basin: Integration of apatite fission track, vitrinite reflectance and biomarker isomerisation analysis: Basin Research, v. 18, p. 27–50, doi:10.1111/j.1365-2117.2006.00286.x.

Mock, S., von Hagke, C., Schlunegger, F., Dunkl, I., and Herwegh, M., 2019, Late Miocene thrusting in the North Alpine foreland: Driven by a deep-seated process and shaped by the local mechanical stratigraphy: Solid Earth Discussions, p. 1–32, doi:10.5194/se-2019-56.

Müller, I.A., Fernandez, A., Radke, J., van Dijk, J., Bowen, D., Schwieters, J., and Bernasconi, S.M., 2017, Carbonate clumped isotope analyses with the long-integration dual-inlet (LIDI) workflow: scratching at the lower sample weight boundaries: Rapid Communications in Mass Spectrometry, v. 31, p. 1057–1066, doi:10.1002/rcm.7878.

Nemcok, M., Schamel, S., and Gayer, R., 2009, Thrustbelts. Structural Architecture, Thermal Regimes and Petroleum Systems: Cambridge University Press, 556pp p., doi:10.1017/CBO9780511584244.

Ortner, H., Aichholzer, S., Zerlauth, M., Pilser, R., and Fügenschuh, B., 2015, Geometry, amount, and sequence of thrusting in the Subalpine Molasse of western Austria and southern Germany, European Alps: Tectonics, v. 34, p. 1–30, doi:10.1002/2014TC003550.

Parrish, R.R., Parrish, C.M., and Lasalle, S., 2018, Vein calcite dating reveals Pyrenean orogen as cause of Paleogene deformation in southern England: Journal of the Geological Society, v. 175, p. 425–442, doi:10.1144/jgs2017-107.

Pfiffner, O.A., 1986, Evolution of the north Alpine foreland basin in the Central Alps (Switzerland)., *in* P. A. Allen and P. Homewood ed., Foreland basins, Blackwell Publishing Ltd., Oxford, UK, p. 219–228, doi:10.1002/9781444303810.ch11.

Pfiffner, O.A., 2014, Geology of the Alps: John Wiley & Sons.

Pfiffner, O.A., 2017, Thick-skinned and thin-skinned tectonics: A global perspective: Geosciences (Switzerland), v. 7, doi:10.3390/geosciences7030071.

Philippe, Y., Colletta, B., Deville, E., and Mascle, A., 1996, The Jura fold-and-thrust belt: a kinematic model based on map-balancing, *in* Ziegler, P. and Horvath, F. eds., Peri-Tethys Memoir 2: Structure and Prospects of Alpine Basins and Forelands, Museum National d'Historie Naturelle, 170, p. 235 – 261.

Poblet, J., and Lisle, R.J., 2011, Kinematic evolution and structural styles of fold-and-thrust belts: Geological Society Special Publication, v. 349, p. 1–24, doi:10.1144/SP349.1.

Rittner, M., 2013, U-Pb dating of brittle deformation. Unpublished Doctoral Thesis: Royal Holloway University of London, 270 p., https://pure.royalholloway.ac.uk/portal/en/publications/upb-dating-of-brittle-deformation(aff86bf1-7949-4184-88c1-886cc509dcf2).html.

Roberts, N.M.W., Rasbury, E.T., Parrish, R.R., Smith, C.J., Horstwood, M.S.A., and Condon, D.J., 2017, A calcite reference material for LA-ICP-MS U-Pb geochronology: Geochemistry, Geophysics, Geosystems, v. 18, p. 2807–2814, doi:10.1002/2016GC006784.

Schegg, R., Leu, W., Cornford, C., and Allen, P.A., 1997, New coalification profiles in the Molasse Basin of Western Switzerland: Implications for the thermal and geodynamic evolution of the Alpine Foreland: Eclogae Geologicae Helvetiae, v. 90, p. 79–96.

Smeraglia, L. et al., 2018, Crustal-scale fluid circulation and co-seismic shallow comb-veining along the longest normal fault of the central Apennines, Italy: Earth and Planetary Science Letters, v. 498, p. 152–168, doi:10.1016/j.epsl.2018.06.013.

Smeraglia, L., Fabbri, O., Choulet, F., Buatier, M., Boulvais, P., Bernasconi, S.M., and Castorina, F., 2020, Syntectonic fluid flow and deformation mechanisms within the frontal thrust of a foreland fold-and-thrust belt: Example from the Internal Jura, Eastern France: Tectonophysics, v. 778, p. 228178, doi:10.1016/j.tecto.2019.228178.

Sommaruga, A., Burkhard, M., Laubscher, H., Noack, T., and Diebold, P., 1995, Jura Mountains, *in* Deep Structure of the Swiss Alps, Birkhäuser, Basel, Switzerland, p. 45–63, doi:10.1007/978-3-0348-9098-4_7.

Sommaruga, A., Mosar, J., Schori, M., and Gruber, M., 2017, The Role of the Triassic Evaporites Underneath the North Alpine Foreland: Elsevier Inc., 447–466 p., doi:10.1016/b978-0-12-809417-4.00021-5.

Vermeesch, P., 2018, IsoplotR: A free and open toolbox for geochronology: Geoscience Frontiers, v. 9, p. 1479–1493, doi:10.1016/j.gsf.2018.04.001.

Ziegler, P.A., and Fraefel, M., 2009, Response of drainage systems to Neogene evolution of the Jura fold-thrust belt and Upper Rhine Graben: Swiss Journal of Geosciences, v. 102, p. 57–75, doi:10.1007/s00015-009-1306-4.